Ultra-Small Iron Oxide Doped Polypyrrole Nanoparticles for In Vivo Multimodal Imaging Guided Photothermal Therapy

*Xuejiao Song, Hua Gong, Shengnan Yin, Liang Cheng, Chao Wang, Zhiwei Li, Yonggang Li, Xiaoyong Wang, Gang Liu, and Zhuang Liu**

Recently, near-infrared (NIR) absorbing conjugated polymeric nanoparticles have received significant attention in photothermal therapy of cancer. Herein, polypyrrole (PPy), a NIR-absorbing conjugate polymer, is used to coat ultra-small iron oxide nanoparticles (IONPs), obtaining multifunctional IONP@PPy nanocomposite which is further modified by the biocompatible polyethylene glycol (PEG) through a layer-by-layer method to acquire high stability in physiological solutions. Utilizing the optical and magnetic properties of the yielded IONP@PPy-PEG nanoparticles, in vivo magnetic resonance (MR) and photoacoustic imaging of tumor-bearing mice are conducted, revealing strong tumor uptake of those nanoparticles after intravenous injection. In vivo photothermal therapy is then designed and carried out, achieving excellent tumor ablation therapeutic effect in mice experiments. These results promise the use of multifunctional NIR-absorbing organic-inorganic hybrid nanomaterials, such as IONP@PPy-PEG presented here, for potential applications in cancer theranostics.

1. Introduction

Photothermal therapy (PTT) is able to burn cancer through converting near-infrared (NIR) light energy into heat by using NIR-absorbing agents.[1,2] Compared with traditional cancer treatment methods such as radiotherapy and chemotherapy, PTT is highly effective in tumor ablation and exhibits minimal damage to normal tissues. Currently, a large variety of nanomaterials have been developed as PTT agents, such as different types of gold nanomaterials (e.g., gold nanorods, nanoshells, nanostars, and nanocages)[3–7] and carbon nanomaterials (e.g., carbon nanotubes and graphene),[8–12] as well as a number of other inorganic nanomaterials including CuS nanoparticles,[13,14] Pd nanosheets.[15] Although encouraging in vitro and in vivo PTT therapeutic results have been obtained by using those photothermal nano-agents, the potential long term toxicity of those inorganic nanomaterials, which usually would retain inside the body for long periods of time, has aroused widespread concerns.[16–18] The development of organic photothermal nano-agents has, thus, received significant interests.[19–22] Very recently, a number of groups including ours have reported that NIR-absorbing conjugated polymers, such as polypyrrole (PPy), poly aniline, and poly(3,4-ethylenedioxythiophene) poly(styrenesulfonate) (PEDOT:PSS), after appropriate surface coatings could serve as strong photothermal agents, showing excellent cancer ablation effect both in vitro and in vivo.[19,23–28] Our latest work further demonstrated that those conjugated polymeric nanoparticles could also be used as drug delivery carriers for combined photothermal and chemotherapy.[29,30]

On the other hand, introducing imaging during therapy or, namely, imaging-guided therapy has been proposed to be a promising strategy to greatly improve the treatment efficiency. As for photothermal cancer treatment, imaging-guided therapy would be particularly interesting for the following reasons. 1) Imaging is able to provide usable information about the tumor location, size, and shape, which are necessary to ensure the whole tumor is effectively exposed to the light during PTT treatment. 2) To achieve the highest photothermal ablation effect, the NIR laser irradiation has to be applied when the photothermal agent reaches the highest accumulation in the tumor. The real-time track of the photothermal agent after systemic administration by imaging is therefore important to achieve the optimized therapeutic outcome. 3) Although tumor sizes can be easily measured for subcutaneous tumors before and after PTT is applied for primary tumor modals and, eventually, in real clinical applications, advanced imaging techniques are required to monitor the therapeutic response after treatment.[10,31,32] Therefore, the development of multifunctional theranostic agents with both imaging capability and strong

X. J. Song, H. Gong, Dr. L. Cheng, C. Wang, Z. W. Li, Prof. Z. Liu
Jiangsu Key Laboratory for Carbon-Based Functional Materials & Devices
Institute of Functional Nano & Soft Materials Laboratory (FUNSOM)
Soochow University
Suzhou, Jiangsu, 215123, China
E-mail: zliu@suda.edu.cn
S. N. Yin, Dr. Y. G. Li
Department of Radiology
the First Affiliated Hospital of Soochow University
Suzhou, Jiangsu, 215006, China
X. Y. Wang, Prof. G. Liu
Center for Molecular Imaging and Translational Medicine
School of Public Health
Xiamen University
Xiamen, 361005, China

DOI: 10.1002/adfm.201302463

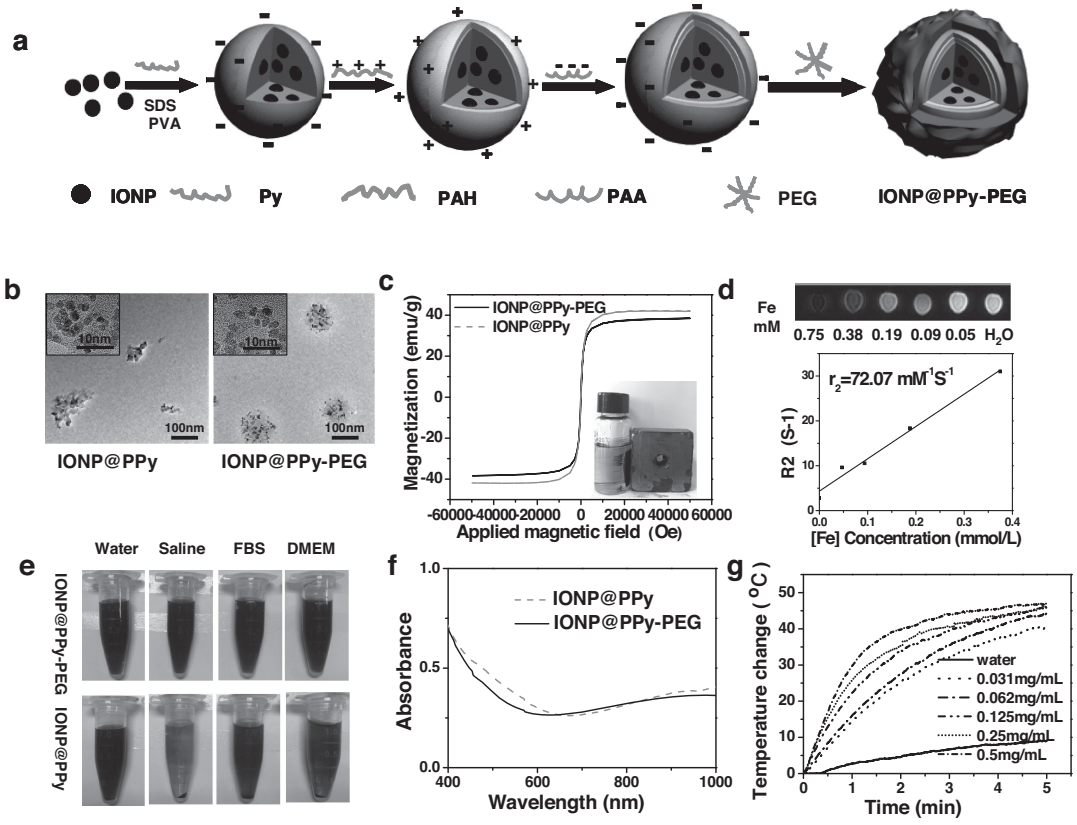

Figure 1. The synthesis and characterizations of IONP@PPy–PEG nanocomposite a) A schematic showing the fabrication process of IONP@PPy–PEG nanocomposite b) TEM images of IONP@PPy nanocomposite before and after PEGylation. Insets are higher resolution images. c) Magnetization loops of IONP@PPy and IONP@PPy–PEG. Inset is a photo of an IONP@PPy–PEG solution placed nearby a magnet. d) T2-weighted MR images (up) and the T2 relaxation rates (R_2) plot (bottom) of IONP@PPy–PEG solutions at different iron concentrations. e) Photos of IONP@PPy and IONP@PPy–PEG in different solutions. Those nanoparticles after PEGylation were stable in those solutions for at least one week without showing obvious aggregation. f) UV–vis–NIR absorbance spectra of IONP@PPy and IONP@PPy–PEG solutions at the same PPy concentration (0.01 mg mL^{-1}). g) Heating curves of pure water and IONP@PPy-PEG solutions of different concentrations under an 808-nm laser irradiation at a power density of 1 W cm^{-2} for 5 min.

NIR absorbance is of great importance for imaging-guided PTT of cancer. Although organic polymeric nanoparticles as the photothermal agents have received significant attention recently,[20–24,29,30,33] the development of multifunctional nanocomposites based on NIR-absorbing conjugated polymer for in vivo multimodal imaging-guided photothermal therapy of cancer upon systemic administration has not yet been reported, to our best knowledge.

In this work, we use polypyrrole (PPy), a NIR-absorbing conjugated polymer, to encapsulate ultra-small iron oxide nanoparticles (IONPs), obtaining multifunctional IONP@PPy nanocomposites with high NIR absorbance and strong superparamagnetism for imaging guided photothermal cancer treatment. In this system, PPy has previous been demonstrated to be non-toxic and not harmful in the area of tissue engineering,[34–36] while various formulations of IONPs have already been proven by U.S. Food and Drug Administration (FDA) as the magnetic resonance (MR) contrast agents for clinical use.[37–41] To offer IONP@PPy water-solubility and physiological stability, those nanoparticles are modified by branched polyethylene glycol (PEG) through a layer-by-layer (LBL) method.[42,43] The obtained IONP@PPy-PEG nanoparticles show no obvious toxicity to several types of cells and appear to be highly effective in photothermal ablation of cancer cells in vitro. Utilizing the magnetic and optical properties of those nanoparticles, in vivo bi-modal MR and photoacoustic imaging are carried out, revealing high tumor accumulation of IONP@PPy-PEG nanoparticles 24 h after intravenous (i.v.) injection. Based on the imaging information, we then design and conduct the in vivo photothermal therapy on tumor-bearing mice, whose tumors are completely eliminated after NIR laser irradiation 24 h post i.v. injection of IONP@PPy-PEG. The mice are tumor-free after treatment, without showing obvious side effect or organ damage within 40 days of observation. Our results suggest that the IONP@PPy–PEG nanocomposite developed in this work may be a promising multifunctional nanoplatform for cancer imaging and therapy.

2. Results and Discussion

The experimental method we used to fabricate IONP@PPy-PEG is shown in **Figure 1**a. We firstly synthesized 6 nm ultra-small IONPs according to the published protocol.[44] The

obtained IONPs were modified by DMSA to increase their water solubility. With IONPs serving as multiple-cores, we used $FeCl_3 \cdot 6H_2O$ as a polymerization inducer, dodecylbenzenesulfonate (SDBS) as an emulsifier, and polyvinyl alcohol (PVA, M.W. 9000–10 000 Da) as a stabilizer, to synthesize PPy coated IONPs (IONP@PPy). From the transmission electron microscopy (TEM) images (Figure 1b), we could see that IONPs were evenly distributed inside PPy nanoparticles, which had an averaged diameter of ≈100 nm. The PPy : IONP weight ratio was estimated to be 1 : 2.2, by calculating the concentration of PPy based on its absorption co-efficient, and measuring the concentration of Fe by inductively coupled plasma atomic emission spectroscopy (ICP-AES).

We then functionalized the as-made IONP@PPy by a LBL polymer coating method. Firstly, negatively charged IONP@PPy nanoparticles were modified by a cationic polymer poly allylamine hydrochloride (PAH) by electrostatic interaction, resulting in a positive charged IONP@PPy/PAH. Secondly, an anionic polyacrylic acid (PAA) polymer was added and cross-linked with the PAH layer by adding N-(3-dimethylaminopropyl-N′-ethylcarbodiimide) hydrochloride (EDC) to trigger amide formation. The zeta potential of those nanoparticles changed from –20 mV to +35 mV after PAH encapsulation, and then back to –40 mV after PAA encapsulation. Lastly, an amine-terminated six-arm branched PEG was conjugated to surface carboxyl groups on IONP@PPy/PAH/PAA nanoparticles via amide formation, obtaining IONP@PPy-PEG used in our following experiments. After PEGylation, the zeta potential of nanoparticles showed an obvious increase to –12.5 mV, due to the consummation of carboxyl groups in the PAA layer and the introduction of amino groups on the branched PEG (Supporting Information, Figure S1a). On the other hand, the hydrodynamic sizes of nanoparticles gradually enlarged as more layers of polymer coatings were added (Supporting Information, Figure S1b). All these results convinced successful coating of different polymer layers on IONP@PPy composite-nanoparticles. Interestingly, after PEGylation of IONP@PPy, the size and morphology of nanoparticles became more uniform, indicating that the LBL polymer coatings might be able to re-shape those nanoparticles by restricting the distortion of PPy in the aqueous phase.

The magnetic properties of IONP@PPy-PEG nanoparticles were then studied. The absence of a hysteresis loop in the field-dependent magnetization measurement illustrated the superparamagnetic nature of our nanocomposite (Figure 1c). In addition, T2-weighted MR images of a series of concentrations of IONP@PPy-PEG solutions acquired by a 3-T MR scanner revealed the concentration-dependent darkening effect. The transverse relaxivity (r_2) of IONP@PPy-PEG was calculated to be 72.07 L $mmol^{-1}$ S^{-1}(Figure 1d).

The PEGylated IONP@PPy exhibited excellent stability in biological mediums, including saline, fetal bovine serum (FBS), and cell medium, allowing those nanoparticles to be further used in biological systems (Figure 1e). IONP@PPy after PEGylation maintained high absorption in the NIR region (Figure 1f). In order to further prove the potential use of IONP@PPy-PEG as a PTT agent, IONP@PPy-PEG solutions of different concentrations were exposed to an 808-nm NIR laser at a power density of 1 W cm^{-2} for 5 min. When exposed to the laser, the temperature of the IONP@PPy-PEG solution even at a low concentration rapidly increased, while pure water showed little temperature change (Figure 1g).

Before conducting the cell related experiments, we studied in vitro cytotoxicity of IONP@PPy-PEG via the standard cell viability MTT assay for 4T1 cells and U937 cells. It was found that IONP@PPy-PEG exhibited little toxicity to cells even under high concentrations after 48 hours of incubation (**Figure 2**a,b). In order to demonstrate the photothermal effect of IONP@PPy-PEG at the cellular level, we tested the nanoparticle concentration-dependent as well as laser power density-dependent photothermal cancer cell killing (Figure 2c,d). As expected, the relative viabilities of cells decreased as we increased the concentration of IONP@PPy-PEG under the same power density of laser. Increasing the laser power density would also result in enhanced photothermal ablation of cancer cells as evidenced by both MTT assay and Trypan blue stained cell images. When treated with the laser at 2 W cm^{-2}, almost all the cells were effective killed (Figure 2e). These data put together proved that our IONP@PPy-PEG nanoparticle could be an effective PTT agent.

Utilizing both magnetic and optical properties of IONP@PPy-PEG, we then carried out in vivo bi-modal imaging on tumor-bearing mice. After been intravenously (i.v.) injected with IONP@PPy-PEG (0.2 mL, 0.8 mg mL^{-1}), MR images of 4T1 tumor-bearing mice revealed the dramatic darkening effect in the tumor area, which showed obvious T2-weighted contrast just 1 h after injection and became even darker later on (**Figure 3**a). The quantified T2-weighted MR signals in the tumor also showed a gradual decrease over 24 h post injection of IONP@PPy-PEG (as much as 75% of decrease at 24 h), suggesting the high accumulation of those nanoparticles in the tumor likely owing to the enhanced permeability and retention (EPR) effect of cancerous tumors (Figure 3b).

On the other side, PPy with strong NIR absorption could also serve as a contrast agent in photoacoustic imaging, which is based on the photoacoustic effect of light-absorbers and offers remarkably increased imaging depth compared with traditional optical imaging techniques. 24 h after i.v. injection of IONP@PPy-PEG, strong photoacoustic contrast showed up in the tumor, whereas in the untreated mice only big vasculatures in the tumor were visible in the photoacoustic image (Figure 3c). The averaged photoacoustic signals in the tumor was also significantly increased (Figure 3d), again demonstrating the high tumor uptake of IONP@PPy-PEG nanoparticles. The combination of the two types of in vivo imaging contrasting abilities endowed IONP@PPy–PEG with great prospect for imaging guided photothermal therapy.

The effect of PTT depended on the amount of the photothermal agent accumulated in the tumor site. As we have not found a way to track the in vivo distribution of PPy, we took advantage of the iron which can be stained by Prussian-blue in the tissues to find out the distribution of those nanoparticles. After being i.v. injected with IONP@PPy–PEG (0.2 mL of 1 mg mL^{-1} solution for each mouse) for 24 h, mice were sacrificed with major organs collected, sliced, and stained with Prussian-blue. High accumulation of IONP@PPy-PEG in both liver and spleen, which were reticuloendothelial systems known to engulf foreign nanoparticles by macrophage clearance, was observed. The Fe levels in heart, kidney, lung and intestine

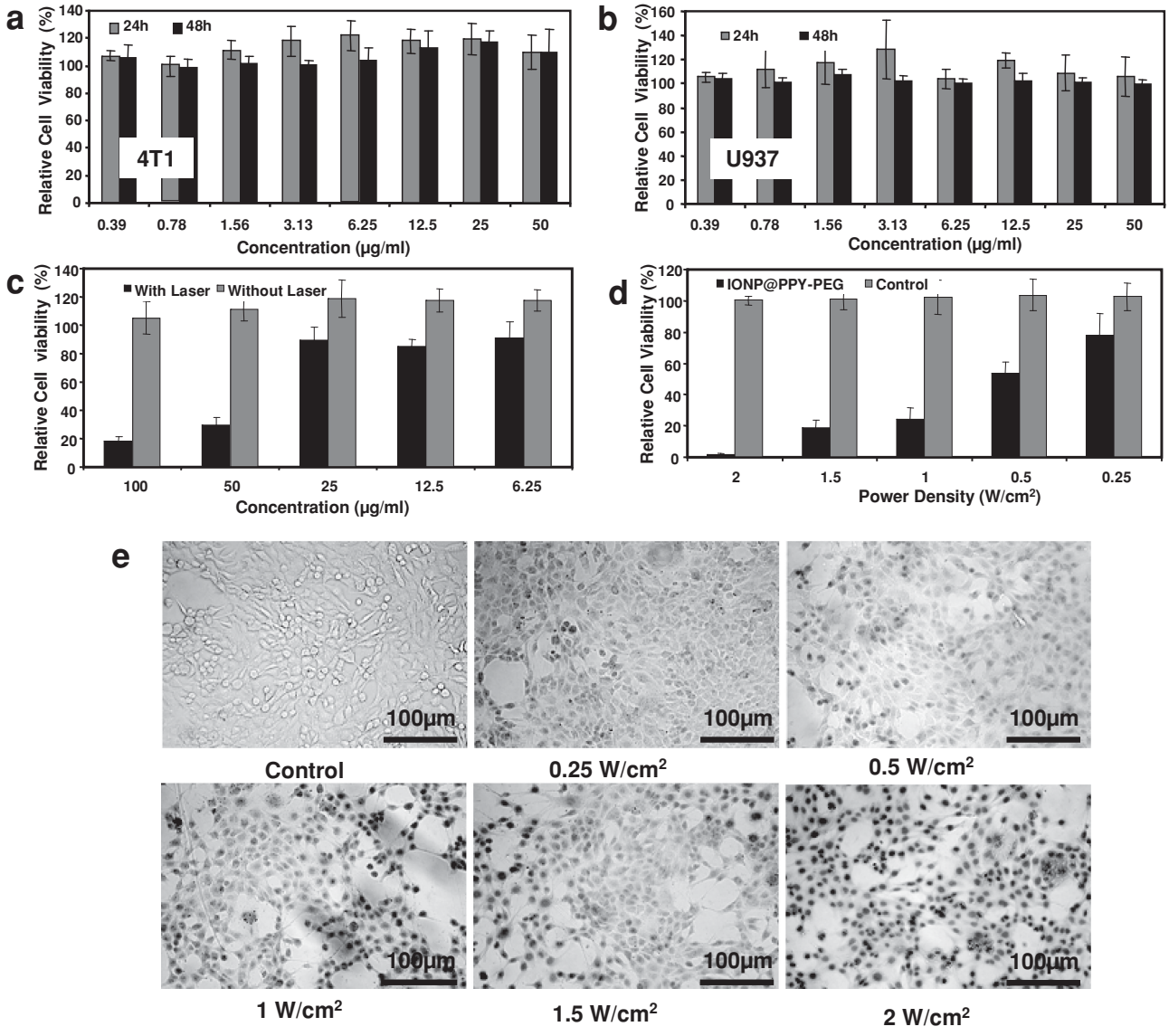

Figure 2. In vitro cell culture experiments. a,b) Cell viability data obtained from the MTT assay of a) 4T1 cells and b) U937 cells incubated with IONP@PPy-PEG at different concentrations. c) Relative viabilities of 4T1 cells treated by IONP@PPy-PEG without and with irradiation by the 808-nm laser (1 W cm^{-2}, 5 min). d) Relative viabilities of 4T1 cells incubated with IONP@PPy-PEG (0.05 mg mL^{-1}) after laser irradiation at different power densities for 5 min. The cell viability values were all normalized to control untreated cells. e) Trypan blue stained images of 4T1 cells incubated with IONP@PPy-PEG (0.05 mg mL^{-1}) after laser irradiation at different power densities for 5 min.

were relatively low (**Figure 4**a). In the tumor, many blue spots could be found, evidencing the rich accumulation of IONP@PPy-PEG nanoparticles in the tumor. In addition, Balb/c mice bearing 4T1 tumors were sacrificed for biodistribution measurement (Figure 4b). It was found IONP@PPy-PEG could passively accumulate in the tumor site (tumor uptake of ≈17%ID g^{-1}). The liver and spleen retention of IONP@PPy-PEG were attributed to the macrophage uptake of nanoparticles in reticuloendothelial systems (RES).

The strong PTT effect of IONP@PPy-PEG shown in the in vitro experiments together with the high tumor accumulation of those nanoparticles as uncovered in our imaging experiments inspired us to use them for in vivo cancer PTT treatment. Female BALB/c mice bearing 4T1 tumors (with diameters of 5–7 nm) were intravenously injected with 200 μL IONP@PPy-PEG at the PPy concentration of 0.8 mg mL^{-1}. 24 h after injection, the mice were exposed to the 808-nm laser irradiation at the power density of 1.5 W cm^{-2} for 5 min. At the same time, PBS injected mice were used as the control group. The temperature change on mice was recorded by an infrared thermal camera during laser irradiation (**Figure 5**a). The surface temperature of the tumor in the treatment group rapidly increased to about 58 °C within 5 min under laser irradiation, while the control group only showed slight increase to about 41 °C. Figure 5b shows representative photos of an IONP@PPy-PEG injected mouse and a PBS injected mouse at day 0 before

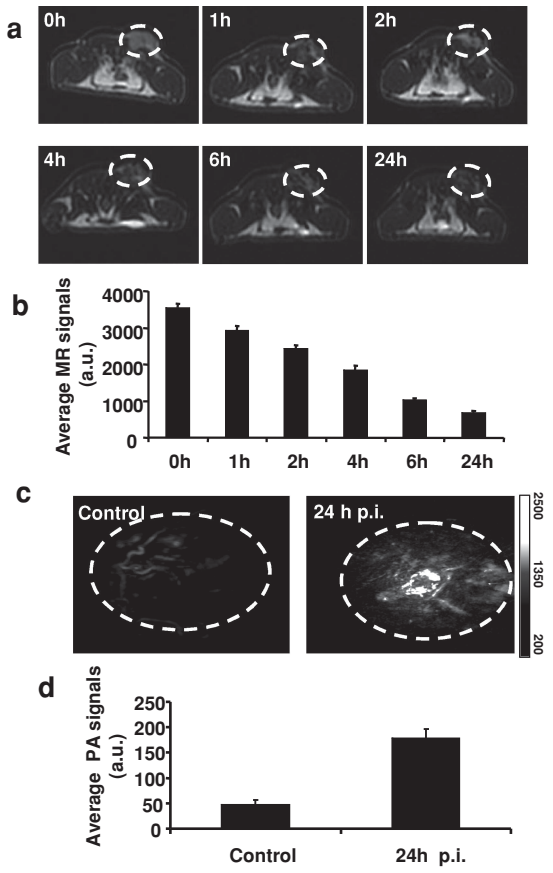

Figure 3. In vivo multimodal imaging. a) T2-weighted MR images of 4T1 tumor-bearing mice i.v. injected with IONP@PPy–PEG (0.8 mg mL^{-1}, 0.2 mL) taken at different time post injection. White circles highlight the tumor site. b) The quantification of T2-weighted MR signals from the tumor at varius time post injection (p.i.) c) Photoacoustic images of mice before injection and at 24 h post injection with IONP@PPy-PEG (0.8 mg mL^{-1}, 0.2 mL). d) The quantification of photoacoustic signals from the tumor site in (c).

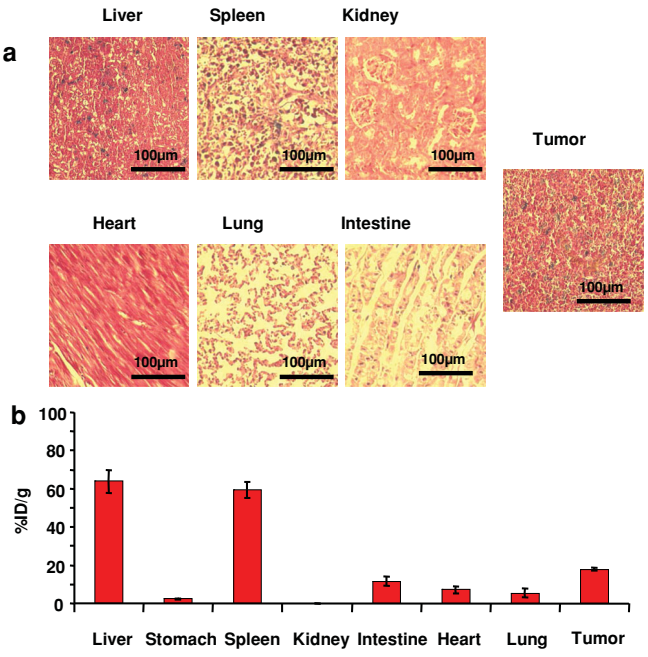

Figure 4. Biodistribution of IONP@PPy-PEG in 4T1 tumor-bearing mice. a) Prussian-blue stained tissue slices of major organs collected from mice 24 h after i.v. injection with IONP@PPy-PEG. b) Biodistribution of IONP@PPy-PEG in 4T1 tumor-bearing mice determined by ICP-measured Fe levels in major organs. High tumor uptake of IONP@PPy–PEG was observed

PTT treatment and at day 2 after treatment. The tumors in the treatment group (IONP@PPy-PEG + laser) were completely burnt, leaving black scars at the original tumor sites which fell off after about 10 d. The tumor sizes of each group were measured by a caliper every other day after treatment (Figure 5c). Tumors on mice injected with IONP@PPy-PEG under laser irradiation disappeared 1 day after treatment, whereas the other groups showed rapid tumor growth. No tumor re-growth was discovered within 40 d. The survival curves of different groups showed that life spans of the mice of the three control groups were no more than 18 days. In marked contrast, mice in the treatment group survived over 40 days without a single death (Figure 5d).

The potential in vivo toxicity of IONP@PPy-PEG was also investigated. We supervised the behaviors of IONP@PPy-PEG-injected Bal/c mice in our experiments after PTT treatment and tumor ablation, noticing no obvious sign of toxic effect within 40 days. Hematoxylin and eosin (H&E) stained images of major organs showed no noticeable organ damage or inflammatory lesion in all major organs of mice 40 days after PTT treatment (Figure 5e). Therefore, our preliminary observation suggested that our PEGylated IONP@PPy nanoparticles were not obviously toxic to the treated animals at our experimental dose.

3. Conclusions

In summary, we have used a LBL method to synthesize PEG modified IONP@PPy with excellent physiological stability, strong superparamagnetism, and high NIR absorbance. Without showing appreciable dark toxicity even at high concentrations, those IONP@PPy-PEG nanoparticles are highly effective in terms of in vitro cancer cell ablation. Based on the inherent magnetic and optical properties of those nanoparticles, tumor-bearing mice after i.v. injection with IONP@PPy-PEG are then imaged by in vivo MR and photoacoustic bi-modal imaging, both of which uncover efficient passive tumor accumulation of IONP@PPy-PEG nanoparticles. Utilizing the strong NIR absorbance and high tumor homing ability of IONP@PPy-PEG, in vivo photothermal cancer treatment is finally carried out, demonstrating great tumor ablation effect with 100% of tumors eliminated after systemic administration of our composite nanoparticles and the followed NIR laser irradiation. Moreover, histological examination reveals no apparent toxicity of IONP@PPy-PEG to mice at our treated dose within 40 days. This work presents a simple approach to prepare multifunctional nanocomposites with great potential in bimodal imaging-guided photothermal therapy of cancer, and encourages further explorations of organic/inorganic nanocomposites for applications in cancer theranostics.

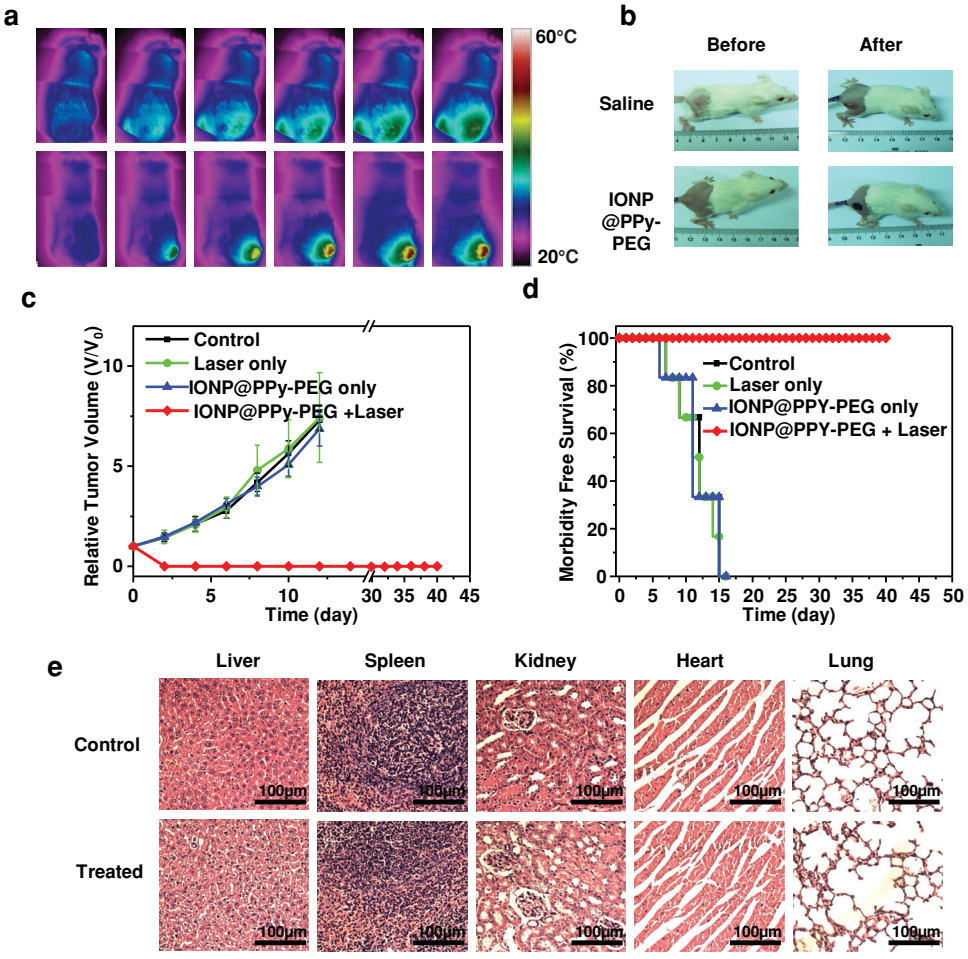

Figure 5. In vivo photothermal therapy using IONP@PPy–PEG. a) Infrared thermal images of 4T1 tumor-bearing mice without (upper row) or with (lower row) i.v. injection of IONP@PPy-PEG (0.8 mg mL^{-1}, 24 h post injection) under 808-nm laser irradiation for 5 min. The laser power density was 1.5 W cm^{-2}. b) Representative photos of saline and IONP@PPy-PEG injected mice taken at day 0 before laser irradiation and at day 2 after PTT treatment. The original tumor turned into a black scar. c) Growth of 4T1 tumors in different groups of mice after various treatments indicated. The relative tumor volumes were normalized to their initial sizes. For the treatment group, six mice injected with IONP@PPy-PEG at 24 h post injection were exposed to the 808-nm laser (1.5 W cm^{-2}, 5 min). The other three groups of mice with six mice per group were used as controls: untreated; laser only; injected with IONP@PPy-PEG but without laser irradiation. d) Survival curves of mice after various treatments indicated. IONP@PPy-PEG injected mice after PTT treatment showed 100% survival ratio over 40 days. e) H&E stained images of major organs from untreated healthy mice and treated mice with IONP@PPy-PEG injection taken 40 days after photothermal therapy (with tumors eliminated). No noticeable abnormality was observed in major organs including liver, spleen, kidney, heart, and lung.

4. Experimental Section

Synthesis of IONP@PPy-PEG: To synthesize IONPs,[44] 4 mmol Fe $(acac)_3$ (Sigma-Aldrich), 20 mmol 1, 2-Dexadecanediol (Sigma-Aldrich), 12 mmol oleic acid (OA, Sigma-Aldrich), 12 mmol oleylamine (OM, Sigma-Aldrich), and 40 mL benzyl ether (Sigma-Aldrich) were mixed and magnetically stirred under the flow of nitrogen. The mixture was heated to 200 °C for 2 h, and then heated to 300 °C for 1 h under a blanket of nitrogen. The black-colored mixture was cooled down to room temperature. Under the ambient condition, ethanol (80 mL) was added to the mixture. The obtained black solid was precipitated, separated via centrifugation, and then dissolved in hexane in the presence of OA and OM. Afterwards the product was precipitated with ethanol, centrifuged to remove the solvent, and re-dispersed into tetrahydrofuran (THF).

To modified as-made IONPs, 20 mg meso-2, 3-Dimercaptosuccinic acid (DMSA, Sigma-Aldrich) was dissolved in 1 mL water containing Na_2CO_3, and slowly added into a THF solution containing 20 mg IONPs under ultrasonication for 30 min to transfer IONPs into the aqueous phase. After stirring at room temperature for 2 h, the solvent was removed by centrifugation at 4800 rpm. The DMSA modified IONPs could be easily dissolved in water with excellent stability.[45]

The Fe_3O_4@PPy composites were synthesized by an in situ chemical oxidative polymerization in the presence of DMAS-modified IONPs. In a typical procedure, 10 mg DMAS-modified IONPs were added into an aqueous solution containing 5 mg dodecylbenzenesulfonate (SDBS, Sigma-Aldrich) and 15 mg polyvinyl alcohol (PVA, Sigma-Aldrich). The solution was then ultra-sonicated to make IONPs well dispersed. Then the solution was stirred at room temperature for 20 min and then added with 20 μL of pyrrole (Sigma-Aldrich) monomer. After further stirring for 30 min, 20 mg $FeCl_3$ solution was dropwisely added into the reaction mixture to induce the polymerization reaction. The mixture was then polymerized for 6 h at room temperature to obtain IONP@PPy core-shell nanocomposites with dark green color.

The synthesized IONP@PPy nanoparticles were negatively charged and modified through a LBL method by electrostatic interaction. First, 10 mg IONP@PPy nanoparticles in water was added into an aqueous solution containing 20 mg of a cationic polymer poly allylamine hydrochloride (PAH, Sigma-Aldrich). After ultrasonication for 30min, the solution was stirred at room temperature for about 6 h and then purified by filtration through 100 kDa molecular weight cut-off (MWCO) filters (Millipore) to remove excess PAH. The obtained IONP@PPy/PAH nanocomposites which were positive charged were added into 10 mL of polyacrylic acid (PAA, Sigma-Aldrich) (4 mg mL^{-1}) solution under ultrasonication for 30min and then stirred for 6 h. After adjusting the pH to 7.4 by a NaOH solution, 10 mg of N-(3-dimethylaminopropyl-N'-ethylcarbodiimide) hydrochloride (EDC, Fluka Inc.) was added into the mixture to induce cross-linking between PAH and PAA layers on the nanoparticles. The reaction was allowed to occur overnight, yielding an IONP@PPy/PAH/PAA solution, from which excess PAA and EDC was removed by filtration through 100 kDa MWCO filters. Lastly, a solution of six-arm PEG-amine (Sunbio Inc. P6AM-10) at the concentration of 5 mg mL^{-1} was added into the IONP@PPy/PAH/PAA solution under sonication for 30 min. 10 mg of EDC was then added into the mixture, whose pH was adjusted to 7.4. The reaction was allowed to sit overnight, yielding an IONP@PPy-PEG solution which was purified by filtration through 100 kDa MWCO filters.

Cellular Experiments: The murine breast cancer 4T1 cell line and the U-937 cell line were originally obtained from American Type Culture Collection (ATCC). All cell culture related reagents were purchased from HyClone. Cells were grown in normal RPMI-1640 culture medium with 10% fetal bovine serum (FBS) and 1% penicillin/streptomycin.

The in vitro cytotoxicity was measured using a standard methyl thiazolyl tetrazolium (MTT, Sigma–Aldrich) assay. 4T1 and U937 cells were seeded into 96-well cell-culture plates at 1×10^4 $well^{-1}$ and then incubated for 24 h at 37 °C under 5% CO_2. After incubating 4T1 and U937 cells with various concentrations of free IONP@PPy-PEG for 24 h and 48 h, the standard MTT assay was carried out to determine the cell viabilities relative to the control untreated cells.

For photothermal cancer cell killing, 4T1 cells were incubated with different concentrations of IONP@PPy–PEG at 37 °C. An 808-nm optical fiber-coupled diode NIR laser (Hi-Tech Optoelectronics Co., Ltd. Beijing, China) was used to irradiate cells at a power density of 1 W cm^{-2} for 5 min. The cell killing efficiency after photothermal ablation was determined by a standard cell viability assay using MTT. For trypan blue staining experiment, 4T1 cells were incubated with 0.05 mg mL^{-1} IONP@PPy-PEG in 35 mm culture dishes. After irradiation by the 808-nm laser at different power densities for 5 min, cells was washed with PBS and stained with 0.04% Trypan blue solution (Sigma Inc.) for 5 min. Microscopic images of cells were then taken using a Leica microscope.

Animal Model: BALB/c mice (≈20 g) were purchased from Nanjing Pengsheng Biological Technology Co, Ltd and used under protocols approved by Soochow University Laboratory Animal Center. For the 4T1 murine breast tumor model, $\approx 5 \times 10^6$ 4T1 cells in ≈60 µL of serum-free RMPI-1640 medium were subcutaneously injected onto the back of each mouse. The mice were used when their tumor volumes approached 60–70 mm^3.

Multimodal Imaging: IONP@PPy–PEG solutions with concentrations ranging from 0.003 to 0.084 mg mL^{-1} of Fe were scanned under a 3-T clinical MRI scanner (Bruker Biospin Corporation, Billerica, MA, USA) at room temperature. The signal intensity was measured within a manually drawn region-of-interest for each sample after acquiring the T2-weighted MR images. Relaxation rates $R2$ ($R2 = 1/T2$) were calculated from T2 values at different iron concentrations.

For in vivo MR imaging, BALB/c mice bearing 4T1 murine breast cancer tumors were intravenously injected with IONP@PPy–PEG (0.2 ml of 1mg mL^{-1} solution for each mouse). MR imaging was conducted on a 3-T clinical MRI scanner equipped with a special coil designed for small animal imaging. Whereas for in vivo photoacoustic imaging, mice i.v. injected with the same dose of IONP@PPy–PEG were imaged before injection and 24 h post injection, by using an Endra Nexus 128 PA imaging system (Endra Inc., Michigan, USA) in the Center for Molecular Imaging and Translational Medicine, Xiamen University.

In Vivo Photothermal Therapy: An optical fiber coupled 808-nm high-power diode-laser (Hi-Tech Optoelectronics Co., Ltd. Beijing, China) was used to irradiate tumors during our experiments. For photothermal treatment, BALB/c mice bearing 4T1 murine breast cancer tumors were i.v. injected with IONP@PPy–PEG (0.2 mL of 1mg mL^{-1} solution for each mouse) at the power density of 1.5 W cm^{-2} for 5 min. Infrared thermal images were taken by an ICI 7320 Pro thermal imaging camera. The tumor sizes were measured by a caliper every other day and calculated as volume = (tumor length) × (tumor width)^2/2. Relative tumor volumes were calculated as V/V_0 (V_0 is the tumor volume when the treatment was initiated).

Tissue Slicing and Staining: BALB/c mice bearing 4T1 murine breast cancer tumors were i.v. injected with IONP@PPy–PEG (0.2 mL of 1 mg mL^{-1} solution for each mouse) and sacrificed at 24 h post injection. Major organs from these mice were collected, fixed in 10% neutral buffered formalin, processed routinely into paraffin, sectioned at 8 µm, stained with Prussian-blue, and examined by a digital microscope (Leica QWin). Examined tissues included liver, spleen, kidney, heart, lung, and intestine and tumor.

Forty days after injection of IONP@PPy-PEG (dose = 10 mg kg^{-1}), three mice from the treatment group and three age-matched female Balb/c control mice (without any injection of IONP@PPy-PEG) were sacrificed. Major organs from these mice were fixed in 10% neutral buffered formalin, processed routinely into paraffin, sectioned at 8 µm, stained with hematoxylin and eosin (H&E), and examined by a digital microscope (Leica QWin). Examined tissues included liver, spleen, kidney, heart, lung, and intestine.

Supporting Information

Supporting Information is available from the Wiley Online Library or from the author.

Acknowledgements

This work was partially supported by the National Natural Science Foundation of China (51222203, 51002100, 51132006), the National "973" Program of China (2012CB932601, 2013CB932702, 2011CB911002), and a Project Funded by the Priority Academic Program Development of Jiangsu Higher Education Institutions. L.C. was supported by a Post-doctoral research program of Jiangsu Province (1202044C).

Received: July 22, 2013
Revised: August 19, 2013
Published online: September 23, 2013

[1] A. M. Gobin, M. H. Lee, N. J. Halas, W. D. James, R. A. Drezek, J. L. West, *Nano Lett.* **2007**, *7*, 1929.
[2] X. H. Huang, I. H. El-Sayed, W. Qian, M. A. El-Sayed, *J. Am. Chem. Soc.* **2006**, *128*, 2115.
[3] J. Chen, D. Wang, J. Xi, L. Au, A. Siekkinen, A. Warsen, Z.-Y. Li, H. Zhang, Y. Xia, X. Li, *Nano Lett.* **2007**, *7*, 1318.
[4] W. Eck, G. Craig, A. Sigdel, G. Ritter, L. J. Old, L. Tang, M. F. Brennan, P. J. Allen, M. D. Mason, *ACS Nano* **2008**, *2*, 2263.
[5] T. Niidome, M. Yamagata, Y. Okamoto, Y. Akiyama, H. Takahashi, T. Kawano, Y. Katayama, Y. Niidome, *J. Controlled Release.* **2006**, *114*, 343.
[6] S. E. Skrabalak, L. Au, X. Lu, X. Li, Y. Xia, *Nanomedicine* **2007**, *2*, 657.
[7] Y. Xia, W. Li, C. M. Cobley, J. Chen, X. Xia, Q. Zhang, M. Yang, E. C. Cho, P. K. Brown, *Acc. Chem. Res.* **2011**, *44*, 914.

[8] J. T. Robinson, S. M. Tabakman, Y. Liang, H. Wang, H. S. Casalongue, V. Daniel, H. Dai, *J. Am. Chem. Soc.* **2011**, *133*, 6825.
[9] K. Yang, S. Zhang, G. Zhang, X. Sun, S.-T. Lee, Z. Liu, *Nano Lett.* **2010**, *10*, 3318.
[10] K. Yang, L. Hu, X. Ma, S. Ye, L. Cheng, X. Shi, C. Li, Y. Li, Z. Liu, *Adv. Mater.* **2012**, *24*, 1868.
[11] M. Li, X. Yang, J. Ren, K. Qu, X. Qu, *Adv. Mater.* **2012**, *24*, 1722.
[12] X. Liu, H. Tao, K. Yang, S. Zhang, S.-T. Lee, Z. Liu, *Biomaterials* **2011**, *32*, 144.
[13] M. Zhou, R. Zhang, M. Huang, W. Lu, S. Song, M. P. Melancon, M. Tian, D. Liang, C. Li, *J. Am. Chem. Soc.* **2010**, *132*, 15351.
[14] Q. Tian, J. Hu, Y. Zhu, R. Zou, Z. Chen, S. Yang, R.-W. Li, Q. Su, Y. Han, X. Liu, *J. Am. Chem. Soc.* **2013**, *135*, 8571.
[15] S. Tang, X. Huang, N. Zheng, *Chem. Commun.* **2011**, *47*, 3948.
[16] G. Jia, H. F. Wang, L. Yan, X. Wang, R. J. Pei, T. Yan, Y. L. Zhao, X. B. Guo, *Environ. Sci. Technol.* **2005**, *39*, 1378.
[17] N. Lewinski, V. Colvin, R. Drezek, *Small* **2008**, *4*, 26.
[18] A. Nel, T. Xia, L. Madler, N. Li, *Science* **2006**, *311*, 622.
[19] Z. Zha, X. Yue, Q. Ren, Z. Dai, *Adv. Mater.* **2012**, *25*, 777.
[20] J. F. Lovell, C. S. Jin, E. Huynh, H. Jin, C. Kim, J. L. Rubinstein, W. C. Chan, W. Cao, L. V. Wang, G. Zheng, *Nat. Mater.* **2011**, *10*, 324.
[21] M. Zheng, C. Yue, Y. Ma, P. Gong, P. Zhao, C. Zheng, Z. Sheng, P. Zhang, Z. Wang, L. Cai, *ACS Nano* **2013**, *7*, 2056.
[22] L. Cheng, W. He, H. Gong, C. Wang, Q. Chen, Z. Cheng, Z. Liu, *Adv. Funct. Mater.* **2013**, DOI: 10.1002/adfm.201301045.
[23] L. Cheng, K. Yang, Q. Chen, Z. Liu, *ACS Nano* **2012**, *6*, 5605.
[24] M. Chen, X. Fang, S. Tang, N. Zheng, *Chem. Commun.* **2012**, *48*, 8934.
[25] J. Yang, J. Choi, D. Bang, E. Kim, E. K. Lim, H. Park, J. S. Suh, K. Lee, K. H. Yoo, E. K. Kim, *Angew. Chem.* **2011**, *123*, 461.
[26] K. Yang, H. Xu, L. Cheng, C. Sun, J. Wang, Z. Liu, *Adv. Mater.* **2012**, *24*, 5586.
[27] L. Feng, C. Zhu, H. Yuan, L. Liu, F. Lv, S. Wang, *Chem. Soc. Rev.* **2013**. *42*, 6620.
[28] H. Chong, C. Nie, C. Zhu, Q. Yang, L. Liu, F. Lv, S. Wang, *Langmuir* **2011**, *28*, 2091.
[29] C. Wang, H. Xu, C. Liang, Y. Liu, Z. Li, G. Yang, L. Cheng, Y. Li, Z. Liu, *ACS Nano* **2013**, *7*, 6782.
[30] H. Gong, L. Cheng, J. Xiang, H. Xu, L. Feng, X. Shi, Z. Liu, *Adv. Funct. Mater.* **2013**, DOI: 10.1002/adfm.201301555.
[31] J. Kim, J. E. Lee, S. H. Lee, J. H. Yu, J. H. Lee, T. G. Park, T. Hyeon, *Adv. Mater.* **2008**, *20*, 478.
[32] U. Lindner, R. A. Weersink, M. A. Haider, M. R. Gertner, S. R. H. Davidson, M. Atri, B. C. Wilson, A. Fenster, J. Trachtenberg, *J. Urol.* **2009**, *182*, 1371.
[33] K. Yang, H. Xu, L. Cheng, C. Sun, J. Wang, Z. Liu, *Adv. Mater.* **2012**, *24*, 5586.
[34] J. H. Collier, J. P. Camp, T. W. Hudson, C. E. Schmidt, *J. Biomed. Mater. Res.* **2000**, *50*, 574.
[35] N. Gomez, C. E. Schmidt, *J. Biomed. Mater. Res. A.* **2007**, *81A*, 135.
[36] J. Y. Lee, C. A. Bashur, A. S. Goldstein, C. E. Schmidt, *Biomaterials* **2009**, *30*, 4325.
[37] L. Bu, J. Xie, K. Chen, J. Huang, Z. P. Aguilar, A. Wang, K. W. Sun, M.-S. Chua, S. So, Z. Cheng, H. S. Eden, B. Shen, X. Chen, *Contrast. Media. Mol. I.* **2012**, *7*, 363.
[38] F. Y. Cheng, C. H. Su, Y. S. Yang, C. S. Yeh, C. Y. Tsai, C. L. Wu, M. T. Wu, D. B. Shieh, *Biomaterials* **2005**, *26*, 729.
[39] R. Hao, R. Xing, Z. Xu, Y. Hou, S. Gao, S. Sun, *Adv. Mater.* **2010**, *22*, 2729.
[40] J. Xie, K. Chen, J. Huang, S. Lee, J. Wang, J. Gao, X. Li, X. Chen, *Biomaterials* **2010**, *31*, 3016.
[41] Q. Xu, L. Zhu, M. Yu, F. Feng, L. An, C. Xing, S. Wang, *Polymer* **2010**, *51*, 1336.
[42] Z. G. Zheng, J. McDonald, R. Khillan, Y. Su, T. Shutava, G. Grozdits, Y. M. Lvov, *J. Nanosci. Nanotechnol.* **2006**, *6*, 624.
[43] D. Khodagholy, T. Doublet, M. Gurfinkel, P. Quilichini, E. Ismailova, P. Leleux, T. Herve, S. Sanaur, C. Bernard, G. G. Malliaras, *Adv. Mater.* **2011**, *23*, H268.
[44] S. Xuan, F. Wang, Y.-X. J. Wang, J. C. Yu, K. C.-F. Leung, *J. Mater. Chem.* **2010**, *20*, 5086.
[45] Y. Liu, J. Wang, *J. Mater. Res.* **2011**, *26*, 822.